© 2000 The Chemical Society of Japan
Bull. Chem. Soc. Jpn., 73, 641—649 (2000)

Photoreduction Processes of α-Dodecamolybdophosphate in Aqueous Solutions: Electrical Conductivity, ^{31}P NMR, and Crystallographic Studies

Eri Ishikawa and Toshihiro Yamase*

Research Laboratory of Resources Utilization, Tokyo Institute of Technology, 4259 Nagatsuta, Midori-ku, Yokohama 226-8503

(Received September 7, 1999)

The photoreduction processes of α-$[PMo_{12}O_{40}]^{3-}$ (α-PMo_{12}(0)) in aqueous solutions at pH 2.0 are discussed on the basis of the results of the electrical conductivities and ^{31}P NMR spectra of photolytes, and the crystal structures of α-type two-electron and β-type four-electron reduction species isolated from photolytes as α-$[(^{i}Pr)_2NH_2]_4[HPMo_{12}O_{40}]\cdot 4H_2O$ (**1**) (α-PMo_{12}(II)) and β-$[(^{i}Pr)_2NH_2]_3[H_4PMo_{12}O_{40}]\cdot 2H_2O$ (**2**) (β-PMo_{12}(IV)): (i) A one-electron reduction species produced by the photoredox reaction of α-PMo_{12}(0) with methanol is degraded to α-B-$[H_3PMo_9O_{31}(OH)_3]^{3-}$ (α-B-PMo_9(0)) and Mo^{V}-containing Mo-triad species (Mo_3). (ii) The formation of the α-type mono-protonated two-electron reduction species, α-$[HPMo_{12}O_{40}]^{4-}$ (α-PMo_{12}(II)), results from the isomerization of the β-type two-electron reduction species, β-$[PMo_{12}O_{40}]^{5-}$ (β-PMo_{12}(II)), which is produced by coupling between the one-electron reduced α-B-PMo_9 (α-B-PMo_9(I)) and Mo_3. (iii) The β-type four-protonated four-electron reduction species, β-$[H_4PMo_{12}O_{40}]^{3-}$ (β-PMo_{12}(IV)) as a final product is produced by the disproportionation of α-PMo_{12}(II). The change in the electrical conductivity of the photolytes during photolysis supports the above processes for the photoreduction of α-$[PMo_{12}O_{40}]^{3-}$ to β-$[H_4PMo_{12}O_{40}]^{3-}$ at pH 2.0.

The α-Keggin structural heteropolyoxomolybdates are hydrolyzed and isomerized to the β-Keggin type species in aqueous solutions.[1] Such a property of the polyoxomolybdates causes the mechanism of their reduction to be more complicated. The electrochemical reduction of α-$[PMo_{12}O_{40}]^{3-}$ in acidic media showed that the β-type two-electron reduction species leads to the formation of the β-type four-electron reduction species.[1] On the other hand, the chemical reduction of α-$[PMo_{12}O_{40}]^{3-}$ by using ascorbic acid and hydroxylamine proceeded up to four electrons, implying that the α-type two-electron reduction species was isomerized to the β-type two-electron reduction species, followed by disproportionation to the β-type four-electron reduced species and the β-type oxidized species. The latter was quickly isomerized to the α-type oxidized species.[2]

In this work, the photochemical reduction of α-$[PMo_{12}O_{40}]^{3-}$ in the presence of methanol (MeOH) as a typical electron donor in aqueous solutions, which yields the β-type four-electron reduction species as a final reduction product, was investigated with the help of the electrical conductivity and ^{31}P NMR spectrum of photolytes, as well as the crystal structural characterization of the α-type two-electron and β-type four-electron reduction products. There has been no mechanistic detail of the photoreduction of α-$[PMo_{12}O_{40}]^{3-}$, especially the reorganization processes of the anion framework after reduction, although it is known that the photoredox reaction of polyoxomolybdates undergoes via electron transfer from MeOH to the O→Mo ligand-to-metal charge transfer triplet states with a resultant formation of formyl radical (·CH_2OH) and one-electron reduced polyoxomolybdate.[3]

So far, crystal structural studies of the Keggin-type reduction species of polyoxomolybdates have been carried out for α-$[HPMo_{12}O_{40}]^{4-}$ (two-electron reduction species prepared by chemical reduction),[4] β-$[H_6PMo_{12}O_{40}]^{-}$, (four-electron reduction species prepared by electrochemical reduction),[5] α-$[H_2AsMo_{12}O_{40}]^{3-}$ (two-electron reduction species prepared by oxidation of $[H_6As_{10}Mo_{24}O_{90}]^{8-}$),[6] β-$[H_4AsMo_{12}O_{40}]^{3-}$ (four-electron reduction species prepared also by oxidation of $[H_6As_{10}Mo_{24}O_{90}]^{8-}$),[6] and the hydrothermally prepared one-, two-, and four-electron reduced dodecamolybdosilicates,[7] β-$[HSiMo_{12}O_{40}]^{4-}$, β-$[H_2SiMo_{12}O_{40}]^{4-}$, and β-$[H_5SiMo_{12}O_{40}]^{3-}$. Unfortunately, all structural details of the reduced species of both dodecamolybdophosphates and -arsenates have been lost due to low quality of the diffraction data and/or a partial disordering of the anion atoms.

Experimental

Preparations and Chemical Analyses of Two- and Four-Electron Reduction Species. α-$H_3[PMo_{12}O_{40}]\cdot nH_2O$ and all other reagents used were of analytical grade and were used without further purification. α-$[^{i}Pr_2NH_2]_4[HPMo_{12}O_{40}]\cdot 4H_2O$ (**1**) and β-$[^{i}Pr_2NH_2]_3[H_4PMo_{12}O_{40}]\cdot 2H_2O$ (**2**) were photochemically prepared and crystallized as follows: α-$H_3[PMo_{12}O_{40}]\cdot nH_2O$ (0.2 g, 0.09 mmol) was dissolved in water (20 cm^3) and MeOH (5 cm^3,

0.12 mmol) was added. The resulting solution (at pH 2.0) in a quartz tube (ϕ = 20 mm) was irradiated for 48 h under an atmosphere of nitrogen using a 500 W superhigh-pressure mercury lamp. Then, [^{i}Pr$_2$NH]·HClO$_4$ (2.0 g, 9.9 mmol) and MeOH (12 cm^3, 0.3 mol) were added to the dark-blue colored photolyte and kept at 277 K. Dark-blue needle-like crystals of **1** were precipitated after 24 h. Found: C, 12.64; N, 3.47; H, 2.46%. Calcd for $C_{24}H_{73}N_4PMo_{12}O_{44}$: C, 12.51; N, 3.19; H, 2.43%.

Similarly, [^{i}Pr$_2$NH]·HClO$_4$ and MeOH were added to the 72 h photolyte. Dark-blue hexagonal crystals of **2** were precipitated after a few days. Found: C, 10.50; N, 2.04; H, 2.85%. Calcd for $C_{18}H_{56}N_3PMo_{12}O_{42}$: C, 9.97; N, 1.94; H, 2.60%.

The content of Mo^V in **1** and **2** was measured under a nitrogen atmosphere by a potentionmetric redox titration with a standard solution of KMnO$_4$. All measurements of the open-circuit voltage of electrode vs. Ag–AgCl reference electrode were performed on a Toa Electronics IM-5S ion meter. The analysis showed that the extents of reduction were 1.9±0.1 and 3.8±0.1 electrons in **1** and **2**, respectively. In conjunction with the results of the elemental analysis, **1** and **2** were formulated as α-[^{i}Pr$_2$NH$_2$]$_4$[HPMo$_{12}$O$_{40}$]·4H$_2$O and β-[^{i}Pr$_2$NH$_2$]$_3$[H$_4$PMo$_{12}$O$_{40}$]·2H$_2$O to maintain the electrical neutrality of compounds, respectively.

The amount of formaldehyde (HCHO) as a final oxidation product in photolytes was determined by means of acetylacetone procedure.[8] All procedures for the colorimetric analysis of HCHO were carried out after decoloration of the Mo^V by oxidation with a standard solution of KMnO$_4$.

Electrical Conductivity and ^{31}P NMR Measurements. The photoreduction progresses of α-12-molybdophosphate were monitored by the electrical conductivities and ^{31}P NMR spectra of photolytes of an aqueous solution containing 4 mmol dm^{-3} H$_3$[PMo$_{12}$O$_{40}$]·nH$_2$O and 4.9 mol dm^{-3} MeOH. A sample solution containing a small amount of D$_2$O (10%) was placed in a cylindrical conductivity cell (5 ml) designed for photolysis and irradiated using a 500 W superhigh-pressure mercury lamp. The electrical conductivity of the photolyte in the conductivity cell was measured at 298±1 K with platinum-black electrodes on a Delica a.c. model 12 K Impedance Bridge (frequency : 10^3 Hz). The photolyte in the conductivity cell was supplied for a ^{31}P NMR spectrum measurement (by a use of ϕ = 5 mm NMR tubes) at 298±1 K on a JEOL AL-300 spectrometer, and referenced externally to 85% H$_3$PO$_4$. All of the ^{31}P NMR spectrum measurements were performed by using a 90° pulse. The spin-lattice relaxation time (T_1/s) of each species was evaluated by using the inversion-recovery method. The scan repetition time was selected to be 5-times larger than the longest T_1 (18.6 s for −6.29 ppm-peak). The data were accumulated at 132 scans (about 3.5 h is taken) to obtain an acceptable signal-to-noise ratio. A line-broadening factor of 1.0 Hz was applied before FT. The concentration of a phosphorus compound in a single peak was evaluated from its peak area by multiplying the height and the full-width half-maximum values on the assumption that the sum of peak areas was equal to the initial concentration of α-[PMo$_{12}$O$_{40}$]$^{3-}$. The instrument integrals could not be used for an accurate qualitative analysis, since the areas of the small peaks were systematically underestimated.

X-Ray Structure Analyses. All of the calculations were carried out on a Micro VAXII computer using the TEXSAN[9] software package. Crystals were sealed in Lindemann glass capillaries. The intensity data were collected on a Rigaku AFC-5 diffractometer with graphite-monochromatized Mo $K\alpha$ radiation (λ = 0.71069 Å) generated at 45 kV and 25 mA. The collection of intensity data for **1** was performed at 275 K using an Oxford Cryostream Cooler version 3.1; the collection for **2** was performed at room temperature. Lorentz-polarization and an absorption correction based on Ψ scans of three reflections[10] were applied. The heavy-atom positions for **1** and **2** were determined by direct methods of SHELXS-86[11] and SAPI-91,[12] respectively. Least-squares and differences syntheses cycles were performed for the determining the remaining non-hydrogen atom positions. The refinement was based on F using full-matrix least-squares with a weighting scheme of $\omega^{-1} = \sigma^2(F)$. The anisotopic temperature factors for **1** were applied to all of the atoms in the cell. The short distances of 0.84(4) Å for N(1)···N-(1^{III}) and 1.17(4) Å for O(8)···O(8^{XIV}) are considered to be due to a disorder over the two atoms, and the N(1) atom and O(8) atom were applied with half-occupancies throughout a structure refinement. Anisotopic temperature factors for **2** were applied to all Mo atoms and the P atom. One of three diisopropyl ammonium cations is disordered, and the positional parameters of seven atoms for it were not refined. A common isotopic temperature factor was applied to the seven non-hydrogen atoms of the disordered cation. Their site occupancies were fixed at 0.5 and refined until they converged. Crystallograhic data have been deposited at the CCDC, 12 Union Road, Cambridge CB2 1EZ, UK and copies can be obtained on request, free of charge, by quoting the publication citation and the deposition numbers CCDC 137471, 137472.

Results

Electrical Conductivities and ^{31}P NMR Spectra of Photolytes. Figure 1 shows the change in the electrical conductivity of the photolyte during the reduction of α-[PMo$_{12}$O$_{40}$]$^{3-}$ (α-PMo$_{12}$(0)). The photoreduction of α-PMo$_{12}$(0) exhibited an increase in the electrical conductivity and the highest value in 2 h photolysis, then a decrease while reaching an initial value (Fig. 1). This behavior suggests that more protonated species were produced along with the photolysis, since the oxidation of MeOH to HCHO involves the liberation of two protons into the solution.

The ^{31}P NMR spectra of the photolytes at several steps of the photolysis are shown in Fig. 2. An unirradiated so-

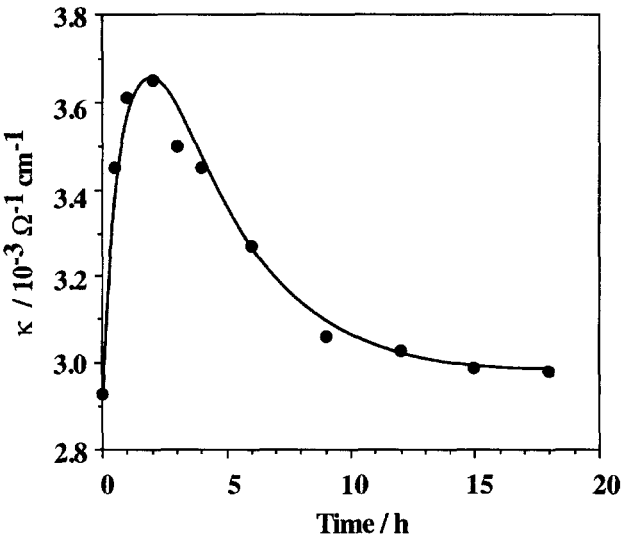

Fig. 1. Plots of the electrical conductivity of the photolyte against the UV-irradiation time (h). Initial concentration of α-PMo$_{12}$(0) and MeOH at pH 2.0 are 4 mmol dm^{-3} and 4.9 mol dm^{-3}, respectively.

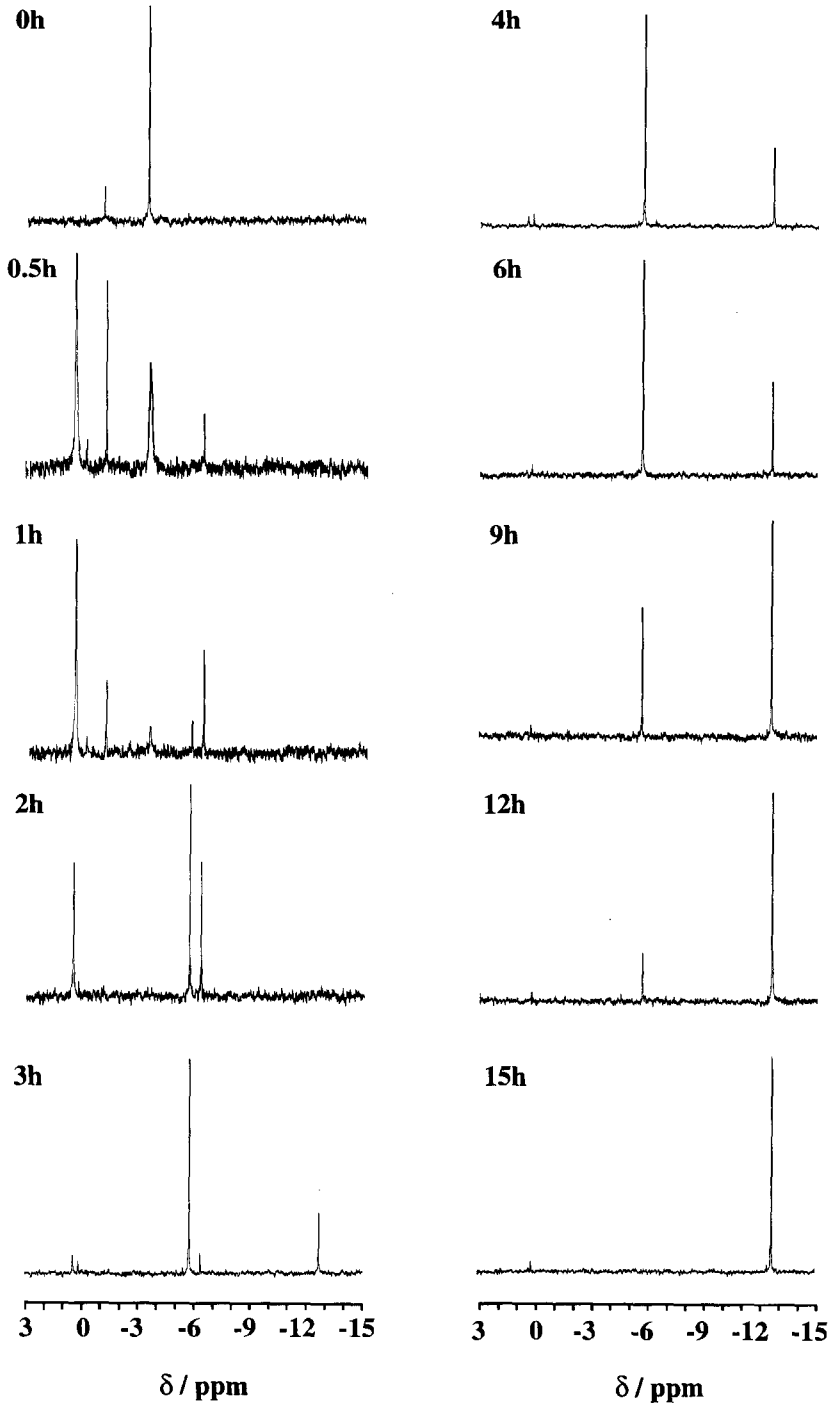

Fig. 2. ^{31}P NMR spectra for the photolysis of α-$PMo_{12}(0)$ at a variety of UV-irradiation time (h). Initial concentrations of α-$PMo_{12}(0)$ and MeOH at pH 2.0 are 4 mmol dm^{-3} and 4.9 mol dm^{-3}, respectively.

lution showed two peaks at -1.07 and -3.42 ppm with relative intensities of 1.0 : 5.7, due to α-$[H_2PMo_{11}O_{39}]^{5-}$ (α-$PMo_{11}(0)$) and α-$PMo_{12}(0)$, respectively.[13] α-$PMo_{11}(0)$ species arises from the degradation of α-$PMo_{12}(0)$ as a result of the partial hydrolysis of α-$PMo_{12}(0)$ in aqueous solutions.[14] At an early stage of the photolysis (in 1 h photolysis), four peaks at 0.54, 0.25, -5.67, and -6.29 ppm appeared. The prolonged photolysis resulted in the appearance of two peaks at 0.25 and -12.62 ppm with an intensity ratio of 1.0 : 12.3, as shown for the 15 h photolyte. The peak at 0.54 ppm has been attributed to the formation of α-B-$[H_3PMo_9O_{31}(OH)_3]^{3-}$ (α-B-$PMo_9(0)$).[13] As described below, the peak species at -5.67 and -12.62 ppm can be identified as the α-type two-electron reduction species, α-$[HPMo_{12}O_{40}]^{4-}$ (α-PMo_{12}(II)), and the β-type four-electron reduction species, β-$[H_4PMo_{12}O_{40}]^{3-}$ (β-PMo_{12}(IV)), respectively, since each chemical shift was consistent with that of crystallographically-characterized corresponding species (as diisopropylammonium salts). The ^{31}P NMR spectra of protonated phosphate ions showed peaks at around 0 ppm

(85% H_3PO_4 reference): for example, the chemical shifts of H_3PO_4,$H_2PO_4^-$ and HPO_4^{2-} in aqueous solutions of 20 mM $NaHPO_4$ are at 0.48, 0.86, and 3.58 ppm, respectively.[15] Therefore, the 0.25 ppm peak (Fig. 2) can be assigned to the species associated with the protonated phosphate species. The peak at −6.29 ppm was assigned to the β-type two-electron reduction species, β-$[PMo_{12}O_{40}]^{5-}$ (β-PMo_{12}(II)), which seemed to be unstable in aqueous solutions, since the chemical shift was close to values of −5.8 ppm in 50% ethanol–water[16] and −6.6 ppm in 50% dioxan–water[2] for β-PMo_{12}(II) species. Although the β-type six-electron reduction species, β-$[PMo_{12}O_{40}]^{9-}$ (β-PMo_{12}(VI)), showed a −6.4 ppm-peak in aqueous solution,[16] the possibility to assign the −6.29 ppm-peak observed in the present system to β-PMo_{12}(VI) is excluded by two facts: (i) the peak at −6.29 ppm was observed at the early stage of photolysis (in 0.5 h photolysis), and (ii) the peak due to β-PMo_{12}(IV) (at −12.62 ppm) was developed with an accompanying depression of the peak of α-PMo_{12}(II) (at −5.67 ppm), which grew from the −6.29 ppm-peak. The peaks at 0.54 and −3.42 ppm during the photolysis are broadened: the broadening of the linewidth for 0.54 ppm-peak gradually decreased from 12.0 to 3.2 Hz with photolysis, while that of the −3.42 ppm-peak increased from 2.8 to 16.0 Hz. Since the other peaks exhibited no significant broadening during photolysis, the line broadening for the α-B-PMo_9(0) and α-PMo_{12}(0) species may be associated with their proximity to the paramagnetic Mo^V species produced by photolysis.

Changes in the concentration of the ^{31}P NMR peak species during photolysis are shown in Table 1, which also shows the presence of 3.7 mmol dm^{-3} β-PMo_{12}(IV) and 0.3 mmol dm^{-3} protonated phosphate ion in the 15 h photolyte (corresponding to the prolonged photolyte in the conductivity cell). On the other hand, prolonged (72 h) photolysis of a solution (25 cm^{-3} in a ϕ = 20 mm quartz tube) containing 4 mmol dm^{-3} α-PMo_{12}(0) and 4.9 mol dm^{-3} MeOH indicated that the amount of HCHO (two-electron oxidized product of MeOH) was 7.5 mmol dm^{-3}, nearly equal to a twofold amount of the initial concentration of α-PMo_{12}(0). Thus, an approximate 1 : 2 relationship between β-PMo_{12}(IV) (3.7 mmol dm^{-3}) and the HCHO concentrations reveals that α-PMo_{12}(0) is photochemically reduced by up to four electrons in the presence of MeOH.[17]

Structure of 1. The addition of 0.4 mol dm^{-3} $[(^iPr)_2NH]\cdot HClO_4$ solids to the 48 h photolyte (25 cm^{-3}) in a ϕ = 20 mm quartz tube, which showed ^{31}P NMR peaks at −5.67, −6.29, and −12.62 ppm with a 4 : 3 : 5 ratio in the peak intensity, led to the formation of single crystals of the α-type two-electron reduction species, **1**, the ^{31}P NMR spectrum of which showed a single peak at −5.63 ppm. The crystal data and condition for the intensity data collection are given in Table 2. Figure 3 shows the anion structure of **1**. The anion of **1** retained α-Keggin structure of the starting oxidized species, α-PMo_{12}(0). The elemental analysis allowed us to formulate **1** as α-$[(^iPr)_2NH_2]_4[HPMo_{12}O_{40}]\cdot 4H_2O$. The highly symmetric space group of the crystal ($P4_2/nmc$, Z = 2) made it impossible to characterize the protonation site within the anion. The structural change by the two-electron reduction was investigated by a comparison with α-$H_3[PMo_{12}O_{40}]\cdot 13$—$14H_2O$.[18] Selected bond lengths, bond angles, and atomic distances of Mo···Mo and Mo···P for **1** are shown in Table 3. The neighboring Mo···Mo distances for edge- and corner-shared MoO_6 octahedra, 3.418(2)—3.429(3) Å (average 3.422(1) Å) and 3.711(2)—3.722(3) Å (average 3.715(1) Å), respectively, are longer than those in the oxidized anion (3.401 Å and 3.699 Å, respectively). Furthermore, the Mo···P distances in **1** (3.5640(8)—3.581(1) Å, average 3.570(1) Å) are slightly larger than for the oxidized anion (3.55 Å). The elongation of the Mo···Mo and Mo···P distances in **1** implies delocalization of two injected electrons over the Keggin-structural Mo_{12} framework of **1**. The asymmetry [1.891(8)—1.893(9) Å (average 1.892(6) Å) and 1.928(3)—1.939(5) Å (average 1.931(3) Å)] of the Mo–O-(μ) distances for the Mo–O(μ)–Mo linkage in **1** drastically decreases, compared to the case (1.86 and 1.96 Å) in the oxidized anion, strongly supporting delocalization of the two injected electrons over the anion.

Structure of 2. Single crystals of the four-electron

Table 1. Amounts (mmol dm^{-3}) of Chemical-Shifts Species in Photolytes for Several Steps of the Photolysis

Irradiation time/h	Chemical-shifts species in photolytes/ppm						
	0.54	0.25	−1.07	−3.42	−5.67	−6.29	−12.62
0			0.6	3.4			
0.5	2.0	0.1	0.5	1.3		0.2	
1.0	2.3	0.1	0.3	0.7	0.2	0.5	
2.0	1.6	0.1			1.4	0.9	
3.0	0.3	0.2			2.6	0.3	0.7
4.0	0.2	0.2			2.6		1.0
6.0		0.2			2.7		1.2
9.0		0.2			1.4		2.4
12.0		0.2			0.8		3.1
15.0		0.3					3.7

a) Amounts (mmol dm^{-3}) of chemical-shift species were calculated with intensity ratio in ^{31}P NMR spectra.

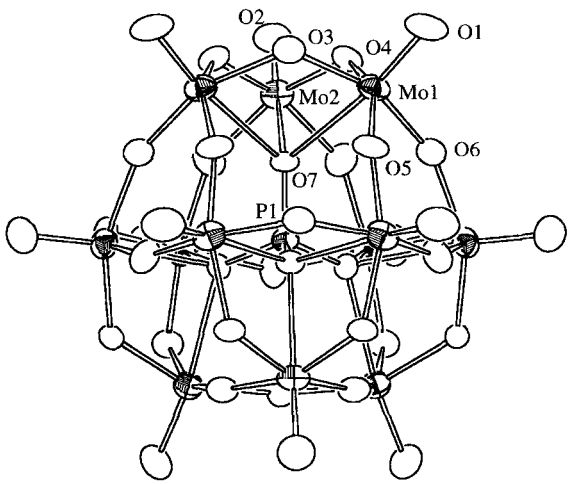

Fig. 3. The structure of the anion for **1**.

Table 2. Crystal Data and Experimental Conditions for the Intensity Data Collection for **1** and **2**

	1	**2**
M_w	2304.09	2200.89
Space group	$P4_2/nmc$	$Pnma$
a/Å	15.227(2)	23.805(4)
b/Å	—	20.543(4)
c/Å	13.409(2)	13.718(2)
V/Å^3	3108.8(5)	6709(2)
Z	2	4
D_c/g cm^{-3}	2.461	2.179
μ/cm^{-3}	24.56	22.64
Crystal size/mm	$0.8\times0.1\times0.1$	$0.3\times0.3\times0.3$
Number of measured reflections	5048	8457
Number of unique reflections	2644	8457
Number of observed reflections ($I>3\sigma(I)$)	961	2848
2θ range	5°—60°	5°—55°
h,k,l range	0, 13/0, 21/0, 18	0, 30/0, 26/ −17, 0
Scan mode	$2\theta/\omega$	$2\theta/\omega$
Scan speed (ω)/° min^{-1}	8	8
Number of parameters	120	151
R	0.050	0.081
R_w	0.034	0.068
Goodness of fit	2.15	3.60
Maximum shift/error	0.002	0.057

Table 3. Selected Bond Lengths (Å), Angles (°), and Other Distances (Å) for **1**

Mo(1)–O(1)	1.655(7)	Mo(2)–O(2)	1.67(1)
Mo(1)–O(3)	1.939(5)	Mo(2)–O(4)	1.891(8)
Mo(1)–O(4)	1.930(8)	Mo(2)–O(6^{XIII})	1.930(9)
Mo(1)–O(5)	1.928(3)		
Mo(1)–O(6)	1.893(9)		
Mo(1)–O(3)–Mo(1^{II})	124.3(5)	Mo(1)–O(4)–Mo(2)	126.8(4)
Mo(1)–O(5)–Mo(1^{III})	149.8(6)	Mo(1)–O(6)–Mo(2^{XIII})	152.2(5)
Mo(1)···Mo(1^{II})	3.429(3)	Mo(1)···Mo(2)	3.418(2)
Mo(1)···Mo(1^{III})	3.722(3)	Mo(1)···Mo(2^{XIII})	3.711(2)
Mo(1)···P(1)	3.5640(9)	Mo(2)···P(1)	3.581(2)
P(1)–O(7)	1.540(9)	O(7)–P(1)–O(7^{III})	110.6(7)
		O(7)–P(1)–O(7^{XIII})	108.9(4)

Symmetry codes: II 3/2−x, y, z; III x, 1/2−y, z; IV 3/2−x, 1/2−y, z; XIII 1−y, 1−x, 1/2−z; XIV 1/2+y, 1−x, 1/2−y; XV 1−y, −1/2+x, 1/2−z; XVI 1/2+y, −1/2+x, −1/2−z.

species, **2**, were isolated from the 72 h photolyte (25 cm^{-3} in a ϕ = 20 mm quartz tube), showing ^{31}P NMR peaks at 0.25 and −12.62 ppm with a 1 : 16 intensity ratio, by adding [(^{i}Pr)$_2$NH]·HClO$_4$ solids (0.4 mol dm^{-3}). The ^{31}P NMR spectra of **2** showed a single peak at −12.66 ppm. Crystal data and the condition for the intensity data collection are also given in Table 2. The anion of **2** displayed the β-Keggin structure with C_{3v} symmetry, indicating 60° rotation of an edge-shared Mo_3O_{13} moiety of the α-Keggin structure around a threefold axis. The twelve Mo atoms in **2** can be classified structurally by three groups: three Mo_{rot} atoms in the 60°-rotated edge-shared Mo_3O_{13} triad, three Mo_{bottom} atoms in the corner-shared Mo_3O_{12} triad on the bottom, and six Mo_{belt} atoms in the central belt Mo_6O_{15} linkage sandwiched by the edge- and corner-shared triads. Figure 4 shows the anion structure (a) β-[$H_4PMo_{12}O_{40}$]$^{3-}$ for **2**, the structural dimensions (b and c) for two kinds of edge-sharing Mo_3O_{13} moieties, and the structural scheme (d) of the corner-shared Mo_3O_{12} triad on the bottom. Selected bond lengths, bond angles and Mo···Mo distances for **2** are listed in Table 4. All of the Mo···Mo distances (3.420(5)—3.555(3) Å) for the edge-shared MoO_6 octahedra in **2** are longer than in α-PMo_{12}(0) (3.401 Å). For the corner-shared MoO_6 octahedra in **2**, the Mo_{rot}···Mo_{belt} (3.642(4)—3.664(5) Å (average 3.653(3) Å)) and Mo_{belt}···Mo_{belt} (3.674(5)—3.681(3) Å (average 3.675(2) Å)) distances are shorter than in the α-PMo_{12}(0) anion (3.699 Å), and the Mo_{bottom}···Mo_{bottom} (3.745(5)—3.808(8) Å (average 3.764(3) Å)) distances are

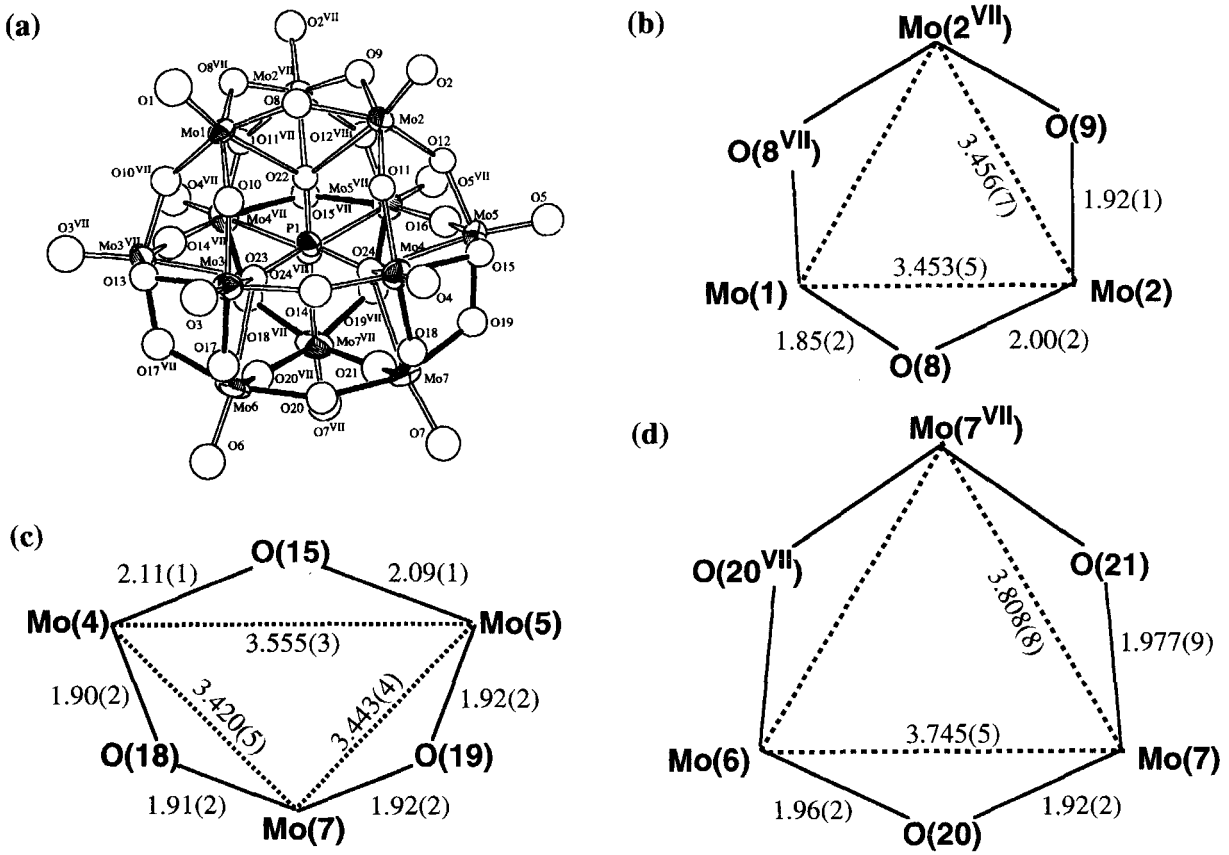

Fig. 4. Schematic representations of the anion for **2**. The structure of β-$[H_4PMo_{12}O_{40}]^{3-}$ (a), the rotated edge-sharing Mo_3O_{13} triad (b), the edge-sharing Mo_3O_{13} triad comprising two Mo_{belt} and one Mo_{bottom} atoms (c), and the corner-sharing Mo_3O_{12} triad on the bottom (d). Filled bonds in (a) indicate the small asymmetry of Mo–O(μ) bonds for the Mo–O(μ)–Mo linkage. Numbers in (b)–(d) indicate atomic distances (Å).

longer. A decrease in the asymmetry of the Mo–O(μ) bond lengths for the Mo–O(μ)–Mo linkage was observed only for the linkages indicated by filled bonds (Fig. 4(a)). The Mo_{belt}–O(μ) bond lengths (2.04(1)—2.11(1) Å, average 2.09(1) Å)) for the edge-sharing Mo_{belt}–O(μ)–Mo_{belt} linkage are elongated, and the Mo–O(μ) bond lengths for the edge-sharing Mo_{belt}–O(μ)–Mo_{bottom} and the corner-sharing Mo_{bottom}–O(μ)–Mo_{bottom} linkages range over 1.90(2)—1.977(9) Å. On the other hand, the Mo–O(μ) asymmetry for both the edge-sharing Mo_{rot}–O(μ)–Mo_{rot} linkages and the corner-sharing Mo_{belt}–O(μ)–Mo_{belt} linkages in **2** is large: 1.88(2)/1.92(2)—1.85(2)/2.00(2) Å (average 1.86(1)/1.95(1) Å), which is close to that of (1.86/1.96) α-$PMo_{12}(0)$. This is a contrast to the case of **1**, where all Mo–O(μ)–Mo linkages showed a decrease due to the asymmetry of the Mo–O(μ) bond lengths. The calculation of bond valence sums[19] indicated that three oxygen atoms (O(13), O(15), and $O(15^{VII})$) (1.08(4)—1.18(4))) at the edge-sharing linkages in the central belt and O(21) (1.48(4)), which is involved in the Mo_3O_{12} triad on the bottom, are protonated. The rest of the bridging oxygen atoms gave large values of the valence sums, 1.7(1)—2.07(3) (average 1.8(1)). The Mo_{belt}–O(μ)–Mo_{belt} bond angles (115.9(7)—119.8(9)°, average 117.2(1)°) for the edge-shared MoO_6 octahedra in the belt are extremely small and those (157(1)°) for the corner-shared MoO_6 octahedra extremely large, compared to the α-$PMo_{12}(0)$ showing 125° and 152° for the edge-shared and corner-shared MoO_6 octahedra respectively. On the other hand, the Mo_{rot}–O(μ)–Mo_{rot} and Mo_{belt}–O(μ)–Mo_{bottom} bond angles for the edge-shared MoO_6 octahedra are 127(1)—128(1)° (average 128(1)°) and the Mo_{rot}–O(μ)–Mo_{belt} and Mo_{bottom}–O(μ)–Mo_{bottom} bond angles for the corner-shared MoO_6 octahedra are 146.6(9)—149(2)° (average 148(1)°), which are close to those for α-$PMo_{12}(0)$.

Discussion

Photoreduction Processes of α-$PMo_{12}(0)$. One might denote that in acetonitrile ^{31}P NMR signals of the α-type one-electron reduction species, (α-$PMo_{12}(I)$) and α-$PMo_{12}(0)$, were observed at 3.5 and −0.4 ppm with linewidths of 2.6 and 0.1 Hz, respectively,[16] and that the 0.54 ppm signal in the present system may be assigned to α-$PMo_{12}(I)$. The fact that the 0.54 ppm signal is observed even in long-term photolysis (until 4 h), however, allowed us to assign the 0.54 ppm signal to α-B-$PMo_9(0)$ in agreement with the ^{31}P NMR result of the MoO_4^{2-}/HPO_4^{2-} system.[15] It is possible to say that the formation of α-B-$PMo_9(0)$ arises only from the photoreduction of α-$PMo_{12}(0)$, since the ^{31}P NMR spectrum of the stock solution of α-$PMo_{12}(0)$ showed no degradation to α-B-PMo_9 (for 48 h in the dark). This let us deduce that

Table 4. Selected Bond Lengths (Å), Angles (°) and Other Distances (Å) for **2**

Mo(1)–O(1)	1.63(3)	Mo(2)–O(2)	1.68(2)	Mo(3)–O(3)	1.65(2)
Mo(1)–O(8)	1.85(2)	Mo(2)–O(8)	2.00(2)	Mo(3)–O(10)	1.87(2)
Mo(1)–O(10)	1.93(2)	Mo(2)–O(9)	1.92(1)	Mo(3)–O(13)	2.04(1)
Mo(1)–O(22)	2.47(2)	Mo(2)–O(11)	1.88(2)	Mo(3)–O(14)	1.91(2)
		Mo(2)–O(12)	1.97(2)	Mo(3)–O(17)	1.90(2)
		Mo(2)–O(22)	2.46(2)	Mo(3)–O(23)	2.49(2)
Mo(4)–O(4)	1.63(2)	Mo(5)–O(5)	1.64(1)	Mo(6)–O(6)	1.70(3)
Mo(4)–O(11)	1.92(2)	Mo(5)–O(12)	1.83(2)	Mo(6)–O(17)	1.91(2)
Mo(4)–O(14)	1.85(2)	Mo(5)–O(15)	2.09(1)	Mo(6)–O(20)	1.96(2)
Mo(4)–O(15)	2.11(1)	Mo(5)–O(16)	1.875(5)	Mo(6)–O(23)	2.42(2)
Mo(4)–O(18)	1.90(2)	Mo(5)–O(19)	1.92(2)		
Mo(4)–O(24)	2.46(2)	Mo(5)–O(24)	2.48(2)		
Mo(7)–O(7)	1.70(2)	Mo(1)–O(8)–Mo(2)	128(1)	Mo(2)–O(9)–Mo(2^{VII})	128(1)
Mo(7)–O(18)	1.91(2)	Mo(1)–O(10)–Mo(3)	149(1)	Mo(2)–O(11)–Mo(5)	148(1)
Mo(7)–O(19)	1.92(2)			Mo(2)–O(12)–Mo(5)	146.6(9)
Mo(7)–O(20)	1.92(2)	Mo(3)–O(13)–Mo(3^{VII})	119.8(9)		
Mo(7)–O(21)	1.977(9)	Mo(3)–O(14)–Mo(4)	157(1)	Mo(4)–O(15)–Mo(5)	115.9(7)
Mo(7)–O(24)	2.38(2)	Mo(3)–O(17)–Mo(6)	128(1)	Mo(4)–O(18)–Mo(7)	128(1)
Mo(5)–O(16)–Mo(5^{VII})	157(1)			Mo(6)–O(20)–Mo(7)	149(1)
Mo(5)–O(19)–Mo(7)	127(1)				
				Mo(7)–O(21)–Mo(7^{VII})	149(2)
Mo(1)···Mo(2)	3.453(5)	Mo(2)···Mo(2^{VII})	3.456(7)	Mo(3)···Mo(3^{VII})	3.538(5)
Mo(1)···Mo(3)	3.664(5)	Mo(2)···Mo(4)	3.654(4)	Mo(3)···Mo(4)	3.681(3)
		Mo(2)···Mo(5)	3.642(4)	Mo(3)···Mo(6)	3.420(5)
Mo(4)···Mo(5)	3.555(5)	Mo(5)···Mo(5^{VII})	3.674(5)	Mo(6)···Mo(7)	3.745(5)
Mo(4)···Mo(7)	3.420(5)	Mo(5)···Mo(7)	3.443(4)		
Mo(1)···P(1)	3.54(1)	P(1)–O(22)	1.48(3)	O(22)–P(1)–O(23)	110(1)
Mo(2)···P(1)	3.55(1)	P(1)–O(23)	1.55(2)	O(22)–P(1)–O(24)	109(1)
Mo(3)···P(1)	3.615(8)	P(1)–O(24)	1.59(2)	O(23)–P(1)–O(24)	108.9(9)
Mo(4)···P(1)	3.620(2)			O(24)–P(1)–O(24^{VII})	111(1)
Mo(5)···P(1)	3.608(8)				
Mo(6)···P(1)	3.56(1)				
Mo(7)···P(1)	3.56(1)				

Symmetry cordes: VII x, $1/2-y$, z.

the photochemical formation of α-B-PMo_9(0) accompanies the liberation of the edge-shared-Mo_3O_{13}-like trimolybdate species (Mo_3),[20] which contains one Mo^V atom as a result of the decomposition of α-PMo_{12}(I), produced by a photoredox reaction between α-PMo_{12}(0) and MeOH. α-B-PMo_9(0) would undergo a photoredox reaction with MeOH to yield the formation of one-electron reduced α-B-PMo_9 (α-B-PMo_9(I)) and the ·CH_2OH radical. ·CH_2OH radicals with a highly negative oxidation potential successively reduce both α-PMo_{12}(0) and α-B-PMo_9(0) to yield HCHO and a corresponding one-electron reduction species.[17] Since β-PMo_{12}(II) was produced after the formation of α-B-PMo_9(0) (Fig. 2 and Table 1), it is reasonable to assume that the formation of β-PMo_{12}(II) results from coupling between α-B-PMo_9(I) and the Mo^V-containing Mo_3 species. The isomerization of β-PMo_{12}(II) to α-PMo_{12}(II) readily proceeded in aqueous media. The $\beta \rightarrow \alpha$ isomerization of the two-electron reduction species can be related to the low symmetry of the β-form (C_{3v}) compared to the α-form (T_d). Such a chemical instability of the β-form would be compensated by the high extent of protonation with a resultant formation of β-PMo_{12}(IV) as a stable final reduction product. The first-order kinetics of the $\beta \rightarrow \alpha$ isomerization process has been established for β-A-$[PV_3W_9O_{40}]^{6-}$.[22] The ^{31}P NMR spectra of the photolytes for more prolonged photolysis indicate that two species, β-PMo_{12}(IV) and the protonated phosphates, remain after the disappearance of α-PMo_{12}(II). It is clear that the α-PMo_{12}(II) is converted into β-PMo_{12}(IV) in the dark. Figure 5 shows the time effect of the ^{31}P NMR spectrum of an aqueous solution of **1** in the dark. As shown in Fig. 5, the ^{31}P NMR spectra of an aqueous solution of **1** (1.8 mmol dm^{-3}, at pH 1.0 adjusted by $HClO_4$) showed a gradual decrease in the concentration of α-PMo_{12}(II) with an accompanying formation of β-PMo_{12}(IV) and protonated phosphates, reaching a perfect conversion into β-PMo_{12}(IV) and protonated phosphates in an approximately 1 : 1 molar ratio. This suggests that the conversion of α-PMo_{12}(II) to β-PMo_{12}(IV) involves disproportionation and subsequent de-

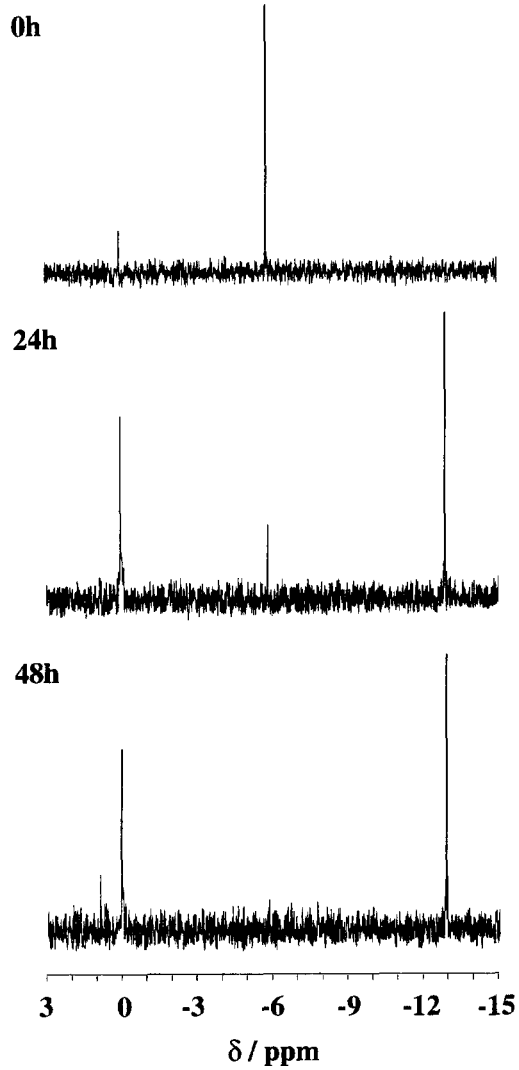

Fig. 5. ^{31}P NMR spectra for the dark reaction of α-PMo_{12}(II) in aqueous solutions. Initial concentration of α-$[(^{i}Pr)_2NH_2]_4[HPMo_{12}O_{40}]\cdot 4H_2O$ at pH 1.0 is 1.8 mmol dm^{-3}.

composition of the oxidized species. In contrast to the above case (Fig. 5), the distribution of the protonated phosphates at the final stage of photolysis is small (ca. 1/10) compared to β-PMo_{12}(IV) (Table 1). Such a contrast seems to be attributed to the difference in the system. Although a further investigation to demonstrate the mechanism of the photolysis of α-PMo_{12}(0) to β-PMo_{12}(IV) is required, there is no doubt that the conversion of α-PMo_{12}(II) to β-PMo_{12}(IV) causes a regeneration of α-PMo_{12}(0) which again undergoes photolysis. Plausible processes for the photolysis of α-PMo_{12}(0) to β-PMo_{12}(IV) are shown in Scheme 1, which are consistent with the above results.

Location of the Injected Electrons. Both swelling of the Mo-atom framework and the small asymmetry on the Mo–O(μ) bond lengths for the Mo–O(μ)–Mo linkage in **1** imply delocalization of the two electrons over the Mo_{12} framework. On the other hand, in **2** both the long Mo···Mo distances for the edge-shared Mo_{belt}–O–Mo_{belt} and Mo_{belt}–O–Mo_{bottom}, and corner-shared Mo_{bottom}–O–Mo_{bottom} linkages and the plausible protonations at O(13), O(15), O(15^{VII}), and O(21) atoms imply the localization of four electrons at three edge-sharing Mo_3O_{13} moieties involving Mo_{belt} and Mo_{bottom} and at the corner-sharing Mo_3O_{12} triad of Mo_{bottom} atoms (Fig. 4(a)). The same is suggested for electrochemically or chemically reduced species: α-$[HPMo_{12}O_{40}]^{4-}$,[4] β-$[H_6PMo_{12}O_{40}]^{-}$,[5] α-$[H_2AsMo_{12}O_{40}]^{3-}$,[6] β-$[H_4AsMo_{12}O_{40}]^{3-}$,[6] and β-$[H_5SiMo_{12}O_{40}]^{3-}$.[7]

Electrical Conductivity of Photolytes. The photoredox reaction of α-PMo_{12}(0) and MeOH allows protons to be liberated in the formation of HCHO as a final oxidation product.[14] The result of an electrical-conductivity measurement of the photolyte showed that the conductivity due to the proton mobility increased until β-PMo_{12}(IV) was produced (2 h photolysis), and decreased with the formation of β-PMo_{12}(IV). X-Ray crystallographic characterizations (Table 2) of **1** and **2** as two-electron reduced mono-proton-

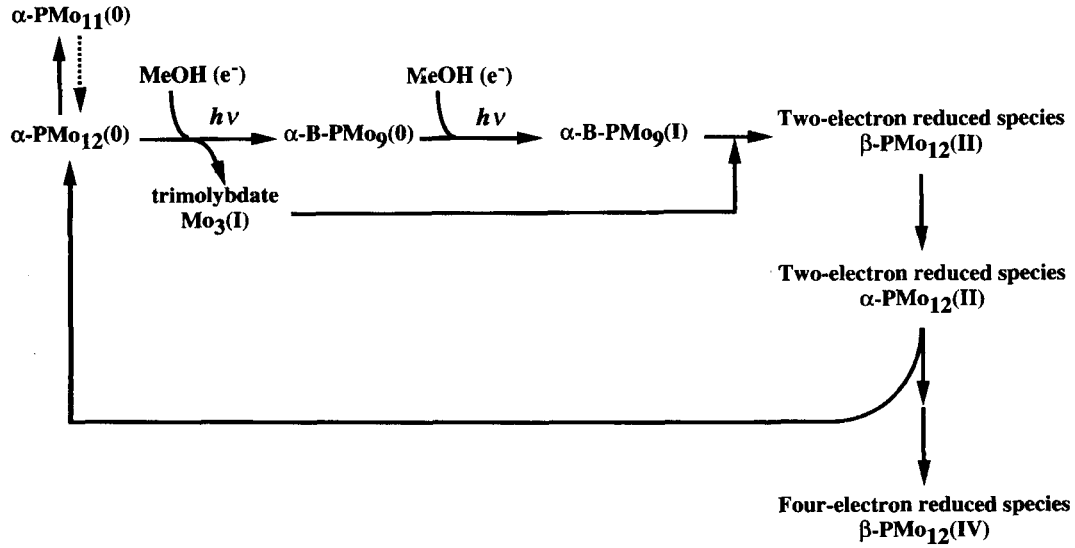

Scheme 1. Proposed processes for the photoreduction of α-PMo_{12}(0) in aqueous solutions.

ated species, α-$[HPMo_{12}O_{40}]^{4-}$, and four-electron reduced four-protonated species, β-$[H_4PMo_{12}O_{40}]^{3-}$, respectively reveals that the increase in the electrical conductivity for the photolyte is due to the formation of the α-PMo_{12}(II) species. In fact, the concentration of the proton liberated in the 2 h photolyte was about 2.3 mmol dm^{-3}, when 350 Ω^{-1} cm^2 $equiv^{-1}$ as the limiting equivalent ionic conductance for protons at 300 K[23] was taken. The value estimated as the liberated proton concentration was approximately comparable to the total concentration of α-PMo_{12}(II) (1.4 mmol dm^{-3}) and β-PMo_{12}(II) (0.9 mmol dm^{-3}) in the 2 h photolyte (Table 1). In conjunction with the estimated values of pK_a for α-PMo_{12}(II) and β-PMo_{12}(II) (2.1 and 2.7, respectively),[1] this suggests that β-PMo_{12}(II) in aqueous solutions at pH 2.0 is also one of the protonated species as well as α-PMo_{12}(II), which is structurally characterized as α-$[HPMo_{12}O_{40}]^{4-}$ (Fig. 3). The formation of β-$[H_4PMo_{12}O_{40}]^{3-}$ as a perfectly proton-compensated species would decrease the conductivity on the conversion of α-PMo_{12}(II) to β-PMo_{12}(IV) (Fig. 5). The fact that the electrical conductivity for the long-term photolysis was close to the one before irradiation (Fig. 1) is in line with the conclusion that the occurrence of the both photoredox reactions of α-PMo_{12}(0) and α-B-PMo_9 with MeOH leads to an almost perfect conversion of α-PMo_{12}(0) to β-PMo_{12}(IV) (Scheme 1).

Supporting Data Available: Atomic coordinates with estimated standard deviations for **1** and **2** are listed in Tables S1 and S2, respectively.[23]

References

1 J. M. Fruchart and P. Souchay, *C. R. Acad. Sci., Ser. C*, **226**, 1571 (1968).

2 J. Aoshima and T. Yamaguchi, *Nippon Kagakukaishi*, **5**, 641 (1986).

3 T. Yamase and K. Ohtaka, *J. Chem. Soc., Dalton Trans.*, **1994**, 2599.

4 R. Neier, C. Trojanowski, and R. Mattes, *J. Chem. Soc., Dalton Trans.*, **1995**, 2521.

5 J. N. Barrows, G. B. Jameson, and M. T. Pope, *J. Am. Chem. Soc.*, **107**, 1771 (1985).

6 A. Müller, E. Krickemeyer, M. Penk, V. Wittneben, and J. Doring, *Angew. Chem., Int. Ed. Engl.*, **29**, 1 (1990).

7 A.Dolbecq, E. Cadot, D. Eisner, and F. Sécheresse, *Inorg. Chem.*, **38**, 4217 (1999).

8 Nippon Yakugakukai, "Eiseishikenhoh Chukai," Kanehara, Tokyo (1973), p. 1065.

9 "TEXSAN, Single-Crystal Structure Analysis Software," Molecular Structure Corporation, The Woodlands, TX (1989).

10 A. C. T. North, D. C. Phillips, and F. S. Mathews, *Acta Crystallogr., Sect. A*, **24A**, 351 (1968).

11 G. Sheldrick, "Structure Analysis Programs with Intelligent Control," Rigaku Corporation, Tokyo (1991).

12 H. -F. Fan, "SAPI 91, Structure Analysis Programs with Intelligent Control," Rigaku Corporation, Tokyo (1991).

13 L. Pettersson, I. Andersson, and L. -O. Öhman, *Inorg. Chem.*, **25**, 4726 (1986).

14 K. Murata and S. Ikeda, *Polyhedron*, **2**, 1005 (1986).

15 L. Pettersson, I. Andersson, and L. -O. Öhman, *Acta Chem. Scand., Ser. A*, **A39**, 53 (1985).

16 J. N. Barrow and M. T. Pope, *Adv. Chem. Ser.*, **226**, 403 (1990).

17 T. Yamase and R. Watanabe, *J. Chem. Soc., Dalton Trans.*, **1986**, 1669.

18 H. D'Amour and R. Allmann, *Z. Kristallogr., Bd.*, **143**, 1 (1976).

19 I. D. Brown and K. K. Wu, *Acta Crystallogr., Sect. B*, **32B**, 1957 (1976).

20 $[Mo^{V}Mo^{VI}_2O_6(H_2O)_7]^{5+}$ is tentatively assumed as a Mo_3 species, what is similar to $[Mo^{IV}_3O_4(H_2O)_9]^{4+}$.[21]

21 D. T. Richens, L. Helm, P. A. Pittet, A. E. Merbach, F. Nicolo, and G. Chapuis, *Inorg. Chem.*, **28**, 1394 (1989).

22 I. Kawafune and G. Matsubayashi, *Bull. Chem. Soc. Jpn.*, **69**, 359 (1996).

23 The aniosotoropic displacement parameters, selected bond distances and angles, and $F_o - F_c$ data are deposited as Document No. 73015 at the Office of the Editor of Bull. Chem. Soc. Jpn.